Geochemical Perspectives Letters

The effect of core segregation on the Cu and Zn isotope composition of the silicate Moon

Y. Xia, E.S. Kiseeva, J. Wade, F. Huang

Supplementary Information

The Supplementary Information includes:

- Petrological Experiments
- Electron Microprobe analysis
- Laser Ablation ICPS analysis
- Isotopic Analysis
- Modelling the Effect of Sulfide Sequestration on the Isotopic Content of the Silicate Moon
- Additional Information in Support of Figure 1
- Figures S-1 to S-4
- Tables S-1 to S-6
- Supplementary Information References

Petrological Experiments

All experiments were performed at 1.5 GPa under fully molten conditions (Table S-1) using a Boyd-England type end-loaded piston-cylinder apparatus at the Department of Earth Sciences, University of Oxford. For all experiments either a $^1/_2$-inch CaF_2 pressure media (for temperatures below 1450 °C) or a $^1/_2$-inch $BaCO_3$–SiO_2 glass (for temperatures 1450 °C and above) assembly with a graphite heater was used (*e.g.*, McDade *et al.*, 2002). The internal spacers consisted of crushable, MgO, fired at 1000 °C to ensure dryness, and the capsule consisted of high density, spectroscopically pure graphite, 6 mm in outer diameter and 3x3 mm inner dimensions. Experimental temperatures were controlled using $W_{95}Re_5$–$W_{74}Re_{26}$ thermocouples separated from the capsule by a 0.5 mm alumina disc. Temperature ranges from 1250 to 1650 °C for sulfide-silicate experiments and 1500 to 1650 °C for metal-silicate experiments (Table S-1). Duration ranged from 30 to 180 min (Table S-1), shown to be adequate for attaining isotope exchange equilibrium at similar P-T conditions (Bridgestock *et al.*, 2014; Mahan *et al.*, 2017). Run durations are varied roughly as a function of temperature, with generally shortened duration at elevated temperature. Experimental products were quenched by cutting power to the resistive furnace whilst run pressure was maintained. During quenching, the experiment cools to beneath the silicate solidus in 2-3 s.

Starting materials were synthetic basalt rock powder, doped with Cu and Zn (Zn as ZnO, Cu as either Cu_2O or Cu_2S), equilibrated with metal or sulfide with variable Ni content (Tables S-2 to S-4), in approximately co-equal mixtures by weight of synthetic sulfide/silicate or metal/silicate. The starting materials were loaded into the graphite capsules; these were found to minimise the potential for Zn loss during the experiment and also aid in the extraction of the run products. Run products were extracted by cutting open the capsule using a diamond wire saw, before setting a small part into epoxy resin prior to polishing for texture and

elemental composition analyses, with the majority used for isotope analysis.

Electron Microprobe Analysis

All experimental products were analysed using a Jeol JXA-8100 electron microprobe using wavelength dispersive spectroscopy (WDS) at the Key Laboratory of Submarine Geosciences, State Oceanic Administration. Analytical conditions were set at 15 kV/20 nA, with a 1 μm spot used for silicate analysis, and 20 kV/20 nA, 10 μm defocused spot utilised for metal and sulfide measurement to better sample areas with heterogeneities. Spectrometers were calibrated for peak position and intensity on a range of natural mineral standards. Peak and background counting time were 10 s for major elements each element. Na, Si, Al, and Mg were run on TAP, K and Ca were run for PETH, Fe, Cr, Mn, Ti, and Ni were analysed on the LIF crystal. Minerals, oxides, pure metals, and pure sulfide were used as standards for all elements. Some samples were repeatedly analysed using a JEOL JXA8600 electron microprobe at the Department of Archaeology at the University of Oxford. WDS analyses were performed using a 15 kV accelerating voltage (15 kV_{acc}) and 20 to 40 nA beam current with a defocused 10-micron beam size. A detailed description can be found in Kiseeva and Wood (2013). Data obtained from the two labs are consistent within error, therefore only the WDS measurements analysed in the Laboratory of Submarine Geosciences are reported. High standard deviations of sulfide phases are due to the heterogeneous quenching of Ni- and Cu- bearing sulfides (Table S-2). The iron bearing experiments (IS7-1, -2, and IS5-2, Fig. S-1) resulted in the metallic component being saturated in carbon. The carbon contents of these experiments were calculated from the Fe-C phases diagram, summarised by Wood, 1993, using the online calculator hosted at http://norris.org.au/expet/metalact/. Major and minor element analysis was performed at Oxford using a Cameca SX5FEG microprobe, 20 kV_{acc} and 20 nA beam, with standards again a range of oxides and metals.

Laser Ablation ICPMS (LA-ICPMS) analysis

Minor and trace element compositions of the quenched silicate melt were determined using an Agilent 7700e ICPMS coupled with a GeolasPro ArF (193 nm) excimer laser sampling system at the Chinese Academy of Sciences Key Laboratory of crust-mantle Materials and Environments, University of Science and Technology of China (USTC), Hefei, China. A calibration strategy of total metal-oxide normalisation (Liu *et al*., 2008) was adopted. Beam diameters of 44 μm were used. More detail about analytical procedures and parameters can be found in He *et al*. (2016). USGS reference glasses possessing comparable compositions with our basaltic silicate glasses including BCR-2, BHVO-1, and BIR-1, were used for external calibration. Analyses of the reference glasses generally agree with the recommended values (https://crustal.usgs.gov/geochemical_reference_standards/microanalytical_RM.html) within 10 % (relative standard deviation, RSD) for minor and trace elements. Compositions for the quenched silicate melt analysed using LA-ICPMS (Table S-4) agree within analytical error those measured by EMPA (Table S-3).

Isotopic Analyses

In previous comparable experiments, no isotopic fractionation of zinc was observed (Bridgestock *et al*., 2014; Mahan *et al*., 2017), mainly due to the relatively large analytical uncertainties caused by error propagation when using the traditional sample-standard bracketing approach (Fig. 2a). To reduce the uncertainty on Zn isotope fractionation, we bracketed the coexisting experimental phases when calculating the isotope fractionation between the two associated silicate and metal/sulfide phases (see Methods). The improved precision (Table S-5) achieved using this method allows clear resolution of the zinc isotope differences between the co-existing phases (Fig. 2a), however, both methods result in fractionation factors that are identical within error (Figs. S-3). For ease of comparison with previously published data we have therefore chosen to use the Cu data derived from the sample-standard bracketing approach.

Chemical purification

The remaining part of each run product was lightly crushed in agate mortar and pestle. Metal, sulfide, and silicate phases were manually separated using optical microscopy and magnets. Cu is both chalcophile and siderophile and Zn is chalcophile and slightly siderophile, such that any contamination from sulfide and metal may alter both the concentration and isotopic signature of the silicate. The silicate fractions were therefore checked for purity with caution by repeating the separation process for several times, and those with magnetic or microscopically visible metal or sulfide were dismissed to minimise cross-contamination for isotope analyses.

The separated phases (silicate, metal, and sulfide fractions) were cleaned prior to digestion to remove any possible surface contamination, by treating with ethanol (3 times, each 15 min), followed by 18.2 MΩ cm Milli-Q H_2O (3 times, each 15 min) in an ultrasonic bath. Dissolution of silicate phase involved three steps using double-distilled, concentrated acids: a 3:1 mixture of HF-

HNO_3; a mixture of HCl-HNO_3; and 1 ml HCl. Metal and sulfide phases were dissolved following the latter two processes. Dissolutions were conducted in closed Savillex beakers on a hot plate at 100 ℃ and were then dried down before the addition of new acids. After full digestion, the samples were dissolved in 6M HCl for major and trace element measurement and column chemistry.

Both purifications of Zn and Cu were achieved by chromatography using anion exchange resin (AG MP–1M, 100–200 mesh), which has high partition coefficients for them at low PH in chloride form. Chemical purification for Zn followed procedures from Chen *et al.* (2016). Samples were dissolved in 1 mL 6M HCl and loaded on to the columns filled with 2 ml resin. Zn was absorbed to the resin as chlorine complex while most other cationic species are eluted with 0.5 HCl. Zn is subsequently eluted using 0.5 N HNO_3. A second separation step with 0.5 ml resin was performed for further purification. Column chemistry of Cu utilised the procedures established by Huang *et al*. (2017). After sample loading onto the column in 1 ml of 6M HCl + 0.001 % H_2O_2, matrix elements were then eluted by 5 ml of 6M HCl + 0.001 % H_2O_2. The Cu was eluted in a further 26 ml of Ml + 0.001 % H_2O_2. The whole procedure was repeated for further purification. Both Cu and Zn yields were checked using ICPMS and proved to be >99.5 %.

Multicollector-ICPMS (MC-ICPMS)

Both Cu and Zn isotopic analyses were performed on a Thermo Scientific Neptune Plus MC–ICPMS in low-resolution mode at USTC. The final sample was dissolved in 2 % HNO_3 and introduced into the instrument using an ESI PFA microflow nebulizer with an uptake rate of (50 μL min^{-1} flow rate). Zinc isotopes were analysed using the techniques described in Chen *et al*. (2016). The yields exceeded 99 %. Isotope ratios are expressed in δ–notation, relative to the NIST SRM 683 standard:

$$\delta^{j/64}Zn_{SRM683} = [(^{j}Zn/^{64}Zn)_{sample} / (^{j}Zn/^{64}Zn)_{SRM683} - 1] \times 1000\ (‰),$$

where j refers to mass 66 or 68. Total procedural Zn and Cu blanks were ca. 5 and <10 ng, respectively, insignificant relative to the amounts of Cu (1-10 μg) and Zn (1-4 μg) onto columns. USGS standards (see Table S-5) were treated along with the samples to test method accuracy. For inter-lab comparison, Zn isotope compositions of USGS standards were calculated as a deviation from JMC–Lyon ($\delta^{j}Zn_{JMC\text{-}Lyon}$) by adding the offset between SRM683 and JMC–Lyon, +0.125 ‰ for $\delta^{66/64}Zn$ and 0.258 ‰ for $\delta^{68}Zn$, based on long-term measurement. Total procedural Zn blank was <10 ng, insignificant relative to the amounts of Zn (1-4 ug) onto columns. Our data for USGS standards (Table S-6) are in excellent agreement with previously published data within error (Moynier *et al*., 2017 and references therein). To assess method reproducibility, several sample aliquots were separated into two parts; each part was separately processed through column chemistry and analyses. These repeats have identical values within error. A number of samples are repeated by dissolving a new quality of powder; again, these re-dissolutions have the sample isotope compositions (Table S-6).

For Cu isotope analyses, ^{63}Cu and ^{65}Cu isotope beams were collected in C and L2 faraday cups, respectively. Matrix elements were monitored using ^{62}Ni and ^{64}Zn beams in L3 and L1 in the same cup setup. Under typical running conditions, a 250 ppb Cu solution generated ca. 5V total signal. To correct for instrumental mass bias, isotope measurements were calculated using the sample standard bracketing protocol relative to the NIST SRM 976 standard, whereby variation in isotopic composition is defined using $\delta^{65/63}Cu$ as follows:

$$\delta^{65/63}Cu = [(^{65}Cu/^{63}Cu)_{sample} / (^{65}Cu/^{63}Cu)_{SRM\,976} - 1] \times 1000\ (‰)$$

Each sample $\delta^{65/63}Cu$ is the average of 3 analyses. Instrumental drift was monitored using two mono-elemental reference materials ERM-AE-647 and AAS, $\delta^{65/63}Cu$ of which are 0.19±0.05 ‰ (2 SD, n= 347) and 0.30± 0.05 ‰ (2SD, n= 51) respectively. Analyses of them yielded a long-term external precision of $\delta^{65/63}Cu$ better than 0.05 ‰ (2 SD, 95 % confidence interval). Total procedural Cu was <5 ng, insignificant relative to the amounts of Cu (1-10 μg) onto columns. Data for USGS standards treated along with the samples agree with previously published data (Moynier *et al.*, 2017 and references therein) within error. Both sample aliquots and sample powder splits exhibit consistent value (Table S-6).

The offset of isotope compositions of the coexisting phases was treated as isotope fractionation factor for Zn and Cu, the uncertainty of which was obtained by error propagation. Specifically, the Zn (or Cu) purified from the coexisting phases were bracketing mutually, acting as standard and sample in the standard bracketing techniques, respectively. The advantage of this technique is that it provides high precision under routine instrument running conditions. Therefore, it provides the possibility to discriminate tiny fractionation approximate analytical error of the traditional method. A similar method was adopted by Pringle and Moynier (2017) to discriminate the slight difference in Rb isotope compositions between the lunar samples and terrestrial rocks by using the terrestrial basalt, BCR-2, as the bracketing standard. The isotope fractionation factor acquired from both methods are identical within error (Tables S-5 and S-6), demonstrating the reliability of our data. The fractionation factor was obtained by linear regression (Figs. 2a & b), of the form $a/T^2+b/T^4$ (T is temperature in kelvin), with model selection made by using that with the lowest BIC (Bayesian information criteria) score.

Modelling the Effect of Sulfide Sequestration on the Isotopic Content of the Silicate Moon

Elemental and isotopic partitioning between silicate and metallic phases is a function of a range of physico-chemical parameters, including temperature, pressure and compositional factors. Lunar formation resulting from a giant impact implies that the pressures of lunar core-mantle differentiation may occur over pressures ranging up to that of the present lunar core mantle boundary (~4.9 GPa) (Righter and Drake, 1996). On the other hand, experimentally derived core-mantle partition coefficients for Cu and Zn are relatively insensitive across the putative pressure range of lunar core formation (*e.g.* Kiseeva and Wood, 2015). For simplicity, the following calculations therefore use a mean core-mantle equilibration pressure of 1.5 GPa, with the advantage that experimentally derived fractionation factors are not affected by the assumed pressures of lunar core formation. Sulfide composition plays a dominant role in setting the elemental partition coefficient, $D^{i}_{sul/sil}$, and temperature determines the isotopic fractionation factor; $\Delta^{i}_{sul/sil}$. $D^{i}_{sul/sil}$ is calculated according to the parameterisation of Kiseeva and Wood (2015), with the BSM FeO content of 9-13 wt. % taken from Wade and Wood (2016) and a normalised terrestrial pyrolite composition taken as the major element composition of the BSM (McDonough and Sun, 1995). We adopt the temperatures of the lunar core formation between 1400 and 1850 ℃, within previously estimated range of 1400 to 1900 ℃ (Righter and Drake, 1996); the silicate melt was fractionally crystallised using Petrolog (Danyushevsky and Plechov, 2011) and the sulfide content of the silicate melt at sulfide saturation calculated using Smythe *et al.* (2017). The temperature dependence of Cu and Zn isotope fractionation factors were calculated (Fig. 2), based on the data derived from the low-Ni experiments, and used to extrapolate the fractionation factor over the full range of temperatures. The size fraction of the lunar core is taken as ~1.6 wt. % by mass (F_{core}) (Weber *et al.*, 2011).

Because extrapolation of the models to temperatures significantly above the experimental range are potentially prone to artefacts (in particular, elevated carbon contents of the metallic phases and ingress of the run products into the capsule), the lunar model presented here is founded on the experimental pressures and temperatures. The models developed here therefore represent minimum lunar core S contents and reinforce the general conclusions of a sulfur rich, carbon deplete lunar core.

Additional Information in Support of Figure 1

The isotopic data shown in Figure 1 was taken from the following sources: Zn (Paniello *et al.*, 2012; Kato *et al.*, 2015), Rb (Pringle and Moynier, 2017), Ga (Kato and Moynier, 2017), K (Wang and Jacobsen, 2016), Cu (Herzog *et al.*, 2009; Savage *et al.*, 2015) and Fe (Craddock *et al.*, 2013; Elardo and Shahar, 2017)

Supplementary Tables

Table S-1 Experimental conditions.

Run #	Starting composition	Doped with elements	Temperature (°C)	Duration (min)
IS5-2	50 % KK3 basalt + 50 % Fe + traces	Cu_2O, ZnO	1650	30
IS7-1	50 % KK3 basalt + 40 % Fe + 10 % Ni + traces	Cu_2O, ZnO	1600	30
IS7-2	50 % KK3 basalt + 40 % Fe + 10 % Ni + traces	Cu_2O, ZnO	1650	30
Cu 2-2	50 % KK3 basalt + 50 % FeS + traces	Cu_2O, NiO	1370	60
Cu 2-3	50 % KK3 basalt + 50 % FeS + traces	Cu_2O, NiO	1430	30
IS3-1	50 % KK3 basalt + 50 % FeS + traces	Ni_3S_2, Cu_2S, ZnO	1500	60
IS3-2	50 % KK3 basalt + 50 % FeS + traces	Ni_3S_2, Cu_2S, ZnO	1600	30
IS4-1	45 % KK3 basalt + 30 % FeS + 20 % Ni_3S_2 + 5 % orthoclase + traces	Cu_2S, ZnO	1400	180
IS4-2	45 % KK3 basalt + 30 % FeS + 20 % Ni_3S_2 + 5 % orthoclase + traces	Cu_2S, ZnO	1350	180
IS4-3	45 % KK3 basalt + 30 % FeS + 20 % Ni_3S_2 + 5 % orthoclase + traces	Cu_2S, ZnO	1300	150
IS4-4	45 % KK3 basalt + 30 % FeS + 20 % Ni_3S_2 + 5 % orthoclase + traces	Cu_2S, ZnO	1250	180
IS4-6	45 % KK3 basalt + 30 % FeS + 20 % Ni_3S_2 + 5 % orthoclase + traces	Cu_2S, ZnO	1500	60
KK54	50 % KK3 basalt + 50 % FeS + traces	Cu_2S, ZnO	1650	30

All runs were conducted at 1.5 GPa.
Graphite capsules were used for all experiments.
KK3 basalt is a synthetic MORB.

Table S-2 Major element compositions (in wt. %) of the metal and sulfide phases measured by EPMA.

Run #	n	Fe	σ	S	σ	Cu	σ	Ni	σ	Zn	σ	Si	σ	total	XC*
IS5-2	46	91.80	0.50	0.04	0.01	2.45	0.23	b.d.l.	-	0.50	0.06	-	-	94.80	0.21
IS7-1	55	77.71	1.55	0.04	0.02	1.37	0.22	15.68	1.28	0.52	0.11	-	-	95.32	0.185
IS7-2	45	75.66	2.07	0.05	0.02	1.27	0.21	17.08	1.56	0.57	0.11	-	-	94.63	0.188
Cu2-2	3	58.31	2.84	32.92	1.48	5.58	2.56	1.10	0.16	-	-	b.d.l.	-	97.91	-
Cu2-3	5	59.65	0.86	33.79	1.01	3.39	1.04	1.24	0.06	-	-	b.d.l.	-	98.07	-
IS3-1	7	62.53	0.37	36.25	0.16	0.41	0.01	0.07	0.02	0.04	0.02	0.03	0.01	99.33	-
IS3-2	9	62.41	0.29	36.19	0.38	0.35	0.03	0.06	0.02	0.05	0.02	0.10	0.06	99.16	-
IS4-1	4	42.48	7.24	32.59	1.31	0.75	0.22	21.41	8.24	-	-	b.d.l.	-	97.25	-
IS4-2	10	35.32	6.15	34.41	3.37	1.94	1.22	26.21	6.30	-	-	b.d.l.	-	98.05	-
IS4-3	8	36.31	3.5	32.45	1.11	1.22	0.46	28.7	4.51	0.13	0.16	0.04	0.01	98.82	-
IS4-4	7	36.85	1.68	32.94	0.89	1.32	0.73	27.94	1.78	0.11	0.19	0.04	0.03	99.21	-
IS4-6	10	35.99	2.88	32.16	1.39	0.98	0.58	29.01	2.93	-	-	0.08	0.05	98.22	-
KK54	11	60.27	1.05	36.73	1.17	0.97	0.14	0.1	0.04	0.15	0.05	0.12	0.04	98.34	-

b.d.l. – below detection limit.

*Mole fraction of carbon in the metallic phase calculated, where present, from the Fe-C phase diagram, summarised by Wood (1993).

For further details, see the online calculator made available at http://norris.org.au/expet/metalact/

Table S-3 Major element compositions (in wt. %) of quenched silicate melt measured by EPMA.

Run #	n	Na_2O	σ	K_2O	σ	SiO_2	σ	Al_2O_3	σ	MgO	σ	CaO	σ	Cr_2O_3	σ	FeO	σ	TiO_2	σ	P_2O_5	σ	ZnO	σ	SO_3	σ	Total	Trace elements*
IS5-2	17	1.78	0.09	0.14	0.01	47.1	0.5	14.74	0.18	10.07	0.16	11.19	0.2	0.01	0.01	10.85	0.38	0.7	0.1	b.d.l.	-	2.55	0.16	0.02	0.01	99.38	0.22
IS7-1	55	2.08	0.09	0.15	0.01	47.16	0.38	15.09	0.09	10.07	0.12	12.01	0.09	-	-	10.28	0.07	0.79	0.02	-	-	2.07	0.03	0.04	0.03	99.95	-
IS7-2	45	2.09	0.09	0.16	0.01	47.88	0.22	15.07	0.09	10.15	0.06	12.05	0.06	-	-	10.13	0.07	0.79	0.02	-	-	2.09	0.03	0.04	0.02	100.65	-
Cu2-2	5	1.75	0.02	b.d.l	-	45.48	0.28	14.43	0.08	9.52	0.05	11.9	0.26	0.07	0.02	15.04	0.12	0.76	0.01	0.14	0.01	n.m.	-	n.m.	-	99.38	0.55
Cu2-3	5	1.71	0.02	b.d.l	-	45.86	0.23	14.37	0.09	9.49	0.05	11.76	0.09	0.08	0.02	15.01	0.1	0.75	0.02	0.13	0.01	n.m.	-	n.m.	-	99.42	0.54
IS3-1	2	1.76	0.04	0.16	0.01	49.29	0.14	14.72	0.11	10.33	0.03	12.28	0.02	0.06	0.03	8.36	0.24	0.83	0.16	0.14	0.01	n.m.	-	n.m.	-	97.99	0.34
IS3-2	19	1.55	0.06	0.14	0.01	48.12	0.25	14.09	0.18	10.32	0.12	11.16	0.22	0.06	0.03	8.2	0.23	0.49	0.09	0.12	0.02	b.d.l.	-	0.72	0.11	95.11	2.83
IS4-1	20	1.76	0.05	1.64	0.03	50.6	0.31	16.07	0.17	9.15	0.08	10.53	0.07	0.04	0.03	7.1	0.17	0.66	0.07	b.d.l.	-	0.87	0.06	0.18	0.01	98.75	0.27
IS4-2	17	1.87	0.05	1.77	0.04	49.38	0.27	16.96	0.19	8.12	0.11	10.62	0.06	0.02	0.02	7.38	0.21	0.7	0.11	b.d.l.	-	1.07	0.05	0.17	0.03	98.25	0.27
IS4-3	15	2.06	0.07	2.21	0.07	50.51	0.2	18.23	0.14	6.49	0.28	8.99	0.14	0.02	0.02	7.28	0.19	0.79	0.11	b.d.l.	-	1.16	0.06	0.15	0.02	98.06	0.28
IS4-4	6	1.75	0.27	1.73	0.42	51.59	0.69	15.16	1.28	8.88	1.69	10.74	1.43	0.06	0.03	7.1	0.09	0.7	0.07	b.d.l.	-	0.84	0.05	0.28	0.17	99.22	0.75
IS4-6	28	1.67	0.05	1.57	0.02	50.71	0.2	15.65	0.11	9.47	0.13	10.99	0.08	0.03	0.03	6.68	0.11	0.58	0.09	b.d.l.	-	0.88	0.05	0.27	0.02	98.66	0.52
KK54	8	1.8	0.05	0.14	0.01	49.41	0.22	15.53	0.15	10.88	0.13	11.94	0.07	0.02	0.01	8.09	0.3	0.64	0.17	b.d.l.	-	0.52	0.05	0.61	0.05	99.71	0.89

* Total trace elements (oxides) derived from LA-ICPMS. EPMA data has been used in preference when above analytical detection limit.

b.d.l. – below detection limit.

n.m. – not measured.

Table S-4 Composition of the quenched silicate melt determined by LA-ICPMS.

Run #	n	MnO wt. %	σ	TiO_2 wt. %	σ	P ppm	σ	Cr ppm	σ	Ni ppm	σ	Cu ppm	σ	Zn ppm	σ	Ba ppm	σ
IS5-2	5	0.1	0.1	0.8	0.1	36	41	44	9	0.2	0.4	813	31	21373	262	58	3
IS7-1	8	0.2	0.2	0.8	0.1	16	22	427	28	110	22	427	28	15588	135	241	4
IS7-2	8	0.2	0.2	0.8	0.1	33	56	406	24	142	12	406	24	15553	424	476	10
Cu2-2	4	0.2	0.2	0.8	0.1	633	44	654	20	19.6	1.8	300	7	564	5	19	1
Cu2-3	4	0.2	0.2	0.8	0.1	570	50	611	10	21.5	1.1	362	6	538	17	17	1
IS3-1	1	0.1	0.1	0.8	0.1	612	-	288	-	3	-	14	-	367	-	57	-
IS3-2	6	0.1	0.1	0.8	0.1	553	135	263	13	0.9	0.6	16	2	344	14	22537	4095
IS4-1	7	0.2	0.2	0.8	0.1	93	108	88	10	206.8	16	28	3	6542	81	19	6
IS4-2	6	0.2	0.2	0.8	0.1	113	66	59	5	195.9	8.8	26	2	8245	187	39	3
IS4-3	2	0.2	0.2	0.9	0.1	121	24	37	3	291.7	185.1	23	4	8743	171	27	1
IS4-4	3	0.2	0.2	0.8	0.1	230	160	157	19	3490.8	317.5	184	9	7356	339	23	3
IS4-6	8	0.2	0.2	0.7	0.1	120	40	106	5	224.7	12.1	31	1	7040	120	2157	545
KK54	3	0.1	0.1	0.8	0.1	200	39	85	7	1.7	1.1	177	23	4176	154	6390	2850
The high-Ba content in IS3-2 glass originated from contamination by the $BaCO_3$ sleeve.																	

Table S-5 Zinc isotope compositions of experimental phases and USGS standards.

Run #	phase	$\delta^{66/64}$Zn (‰)	2SD	$\delta^{68/64}$Zn (‰)	2SD	n	Obtained by sample-standard bracketing				Obtained by sample-sample bracketing			
							$\Delta^{66/64}Zn_{metal/sulfide-silicate}$ (‰)	2SD	$\Delta^{68/64}Zn_{metal/sulfide-silicate}$ (‰)	2SD	$\Delta^{66/64}Zn_{metal/sulfide-silicate}$ (‰)	2SD	$\Delta^{68/64}Zn_{metal/sulfide-silicate}$ (‰)	2SD
IS5-2	silicate	-0.08	0.04	-0.13	0.03	3	0.05	0.05	0.08	0.09	0.03	0.03	0.04	0.08
	metal	-0.03	0.02	-0.05	0.09	3								
IS5-2 rep	silicate	-0.06	0.02	-0.1	0.01	3	0.03	0.02	0.06	0.02	-0.02	0.03	-0.04	0.02
	metal	-0.02	0.00	-0.03	0.01	3								
IS7-1	silicate	-0.005	0.020	-0.001	0.021	3	-0.011	0.032	-0.016	0.053	0.003	0.014	0.005	0.022
	metal	-0.016	0.026	-0.018	0.048	3								
IS7-2	silicate	-0.014	0.016	-0.022	0.021	3	-0.001	0.019	-0.005	0.024	-0.002	0.015	-0.004	0.013
	metal	-0.015	0.010	-0.027	0.012	3								
IS3-1	silicate	0.00	0.01	0.01	0.02	3	-0.15	0.02	-0.29	0.05	-0.17	0.05	-0.29	0.09
	sulfide	-0.15	0.02	-0.28	0.04	3								
IS3-2	silicate	-0.04	0.01	-0.08	0.01	3	-0.09	0.01	-0.16	0.03	-0.07	0.04	-0.13	0.06
	sulfide	-0.13	0.01	-0.25	0.02	3								
KK54	silicate	0.00	0.03	-0.05	0.04	3	-0.07	0.04	-0.05	0.06	-0.05	0.01	-0.11	0.01
	sulfide	-0.06	0.03	-0.11	0.04	3								
IS4-2	silicate	-0.02	0.01	0.01	0.07	3	-0.03	0.03	-0.06	0.09	-0.03	0.02	-0.09	0.09
	sulfide	-0.05	0.03	-0.05	0.06	3								
IS4-3	silicate	-0.02	0.02	-0.04	0.07	3	-0.04	0.05	-0.11	0.21	-0.06	0.03	-0.13	0.04
	sulfide	-0.06	0.05	-0.15	0.2	3								
IS4-4	silicate	-0.03	0.03	-0.06	0.11	3	-0.09	0.04	-0.19	0.11	-0.09	0.01	-0.18	0.08
	sulfide	-0.12	0.01	-0.25	0.03	3								
IS4-6	silicate	-0.03	0.03	-0.04	0.03	3	0.00	0.04	-0.03	0.03	-0.02	0.03	-0.04	0.02
	sulfide	-0.03	0.02	-0.07	0.02	3								
KK54 rep	silicate	-0.03	0.04	-0.03	0.07	3	-0.03	0.06	-0.06	0.11	-0.02	0.03	-0.04	0.02
	sulfide	-0.05	0.04	-0.09	0.08	3								

Table S-5 *Continued*

Run #	phase	$\delta^{66/64}Zn$ (‰)	2SD	$\delta^{68/64}Zn$ (‰)	2SD	n	Obtained by sample-standard bracketing				Obtained by sample-sample bracketing			
							$\Delta^{66/64}Zn_{metal/sulfide-silicate}$ (‰)	2SD	$\Delta^{66/64}Zn_{metal/sulfide-silicate}$ (‰)	2SD	$\Delta^{66/64}Zn_{metal/sulfide-silicate}$ (‰)	2SD	$\Delta^{68/64}Zn_{metal/sulfide-silicate}$ (‰)	2SD
USGS standards														
G-2		0.34	0.05	0.65	0.08	3								
BHVO-2		0.25	0.02	0.53	0.08	3								
AGV-1		0.28	0.02	0.55	0.02	3								
RGM-1		0.33	0.02	0.65	0.02	3								
BCR-2 @1		0.24	0.03	0.48	0.06	3								
BCR-2 @2		0.25	0.03	0.53	0.08	3								
NOD-P		0.8	0.03	1.59	0.04	2								
BIR-1 @1		0.28	0.04	0.57	0.08	2								
BIR-1 @2		0.3	0	0.59	0.02	2								
BIR-1 @3		0.27	0.05	0.55	0.02	2								

"rep" signifies replicate chemical purification and subsequent measurement of the same sample aliquot.

"@" represents independent dissolution, chemical purification, and measurement of powder splits.

Run products and USGS standards are reported as the relative deviation from NIST SRM 683 and JMC-Lyon, respectively.

Table S-6 Copper isotope compositions of experimental phases and USGS standards.

Run #	phase	$\delta^{65/63}$Cu (‰)	2SD	n	Obtained by standard bracketing		Obtained by sample bracketing	
					$\Delta^{65/63}Cu_{metal/sulfide\text{-}silicate}$ (‰)	2SD	$\Delta^{65/63}Cu_{metal/sulfide\text{-}silicate}$ (‰)	2SD
IS5-2	silicate	0.26	0.02	3	0.25	0.03		
	metal	0.51	0.03	3				
IS7-1	silicate	0.25	0.02	3	0.18	0.03		
	metal	0.43	0.02	3				
IS7-2	silicate	0.16	0.04	3	0.07	0.05		
	metal	0.23	0.02	3				
Cu2-2	silicate	0.37	0.02	3	-0.33	0.05		
	sulfide	0.04	0.05	3				
Cu2-3	silicate	0.38	0.02	3	-0.25	0.03		
	sulfide	0.14	0.02	3				
IS3-1	silicate	0.65	0.03	3	-0.23	0.04		
	sulfide	0.42	0.03	3				
IS3-2	silicate	0.56	0.01	3	-0.15	0.02		
	sulfide	0.41	0.02	3				
KK54	silicate	0.65	0.03	3	-0.06	0.05		
	sulfide	0.59	0.04	3				
IS4-1	silicate	0.75	0.03	3	-0.04	0.04	-0.01	0.02
	sulfide	0.71	0.03	3				
IS4-2	silicate	0.70	0.04	3	-0.03	0.06	0.01	0.04
	sulfide	0.67	0.05	3				
IS4-3	silicate	0.72	0.04	3	-0.02	0.06	0.01	0.02
	sulfide	0.70	0.05	3				
IS4-4	silicate	0.79	0.04	3	-0.15	0.06	-0.15	0.02
	sulfide	0.64	0.04	3				

Table S-6 *Continued*

Run #	phase	$\delta^{65/63}$Cu (‰)	2SD	n	Obtained by standard bracketing		Obtained by sample bracketing	
					$\Delta^{65/63}Cu_{metal/sulfide\text{-}silicate}$ (‰)	2SD	$\Delta^{65/63}Cu_{metal/sulfide\text{-}silicate}$ (‰)	2SD
USGS standards								
BCR-2		0.20	0.02	3				
AGV-1 @1		0.04	0.04	3				
AGV-1 @2		0.02	0.04	3				
AGV-1 @3		0.03	0.05	3				
BHVO-2 @1		0.14	0.02	3				
BHVO-2 @2		0.16	0.05	3				
NOD-P @1		0.40	0.03	3				
NOD-P @2		0.41	0.04	3				
NOD-P @3		0.37	0.05	3				
NOD-A		0.30	0.04	3				
BIR-1 @1		0.10	0.04	3				
BIR-1 @2		0.11	0.01	3				

"@" represents independent dissolution, chemical purification, and measurement of powder splits.

Supplementary Figures

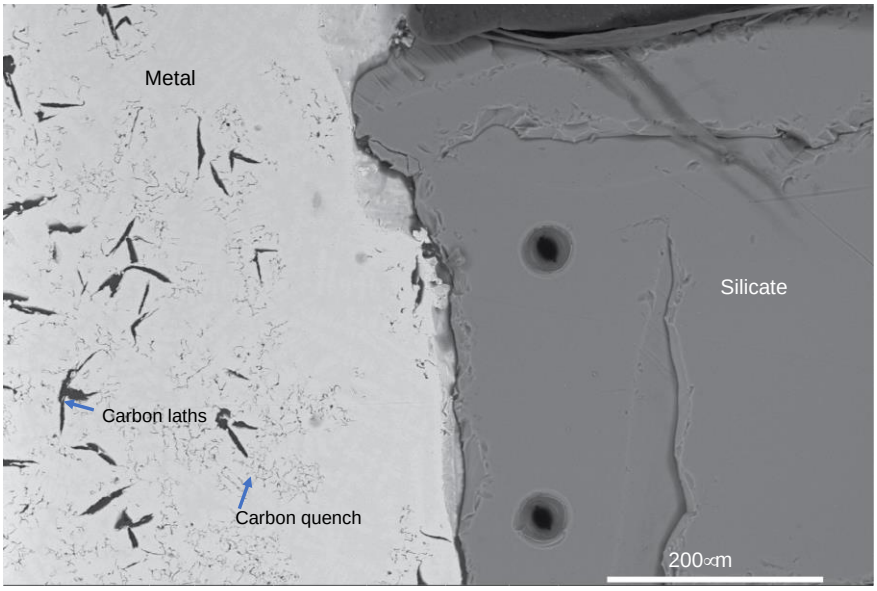

Figure S-1 Backscattered electron (BSE) image of the iron-rich experiment 7-1, showing the carbon-rich metallic phase (left), with both precipitated carbon laths and exsolved carbon quench, and the silicate phase (right). Holes in the silicate portion are laser ablation pits.

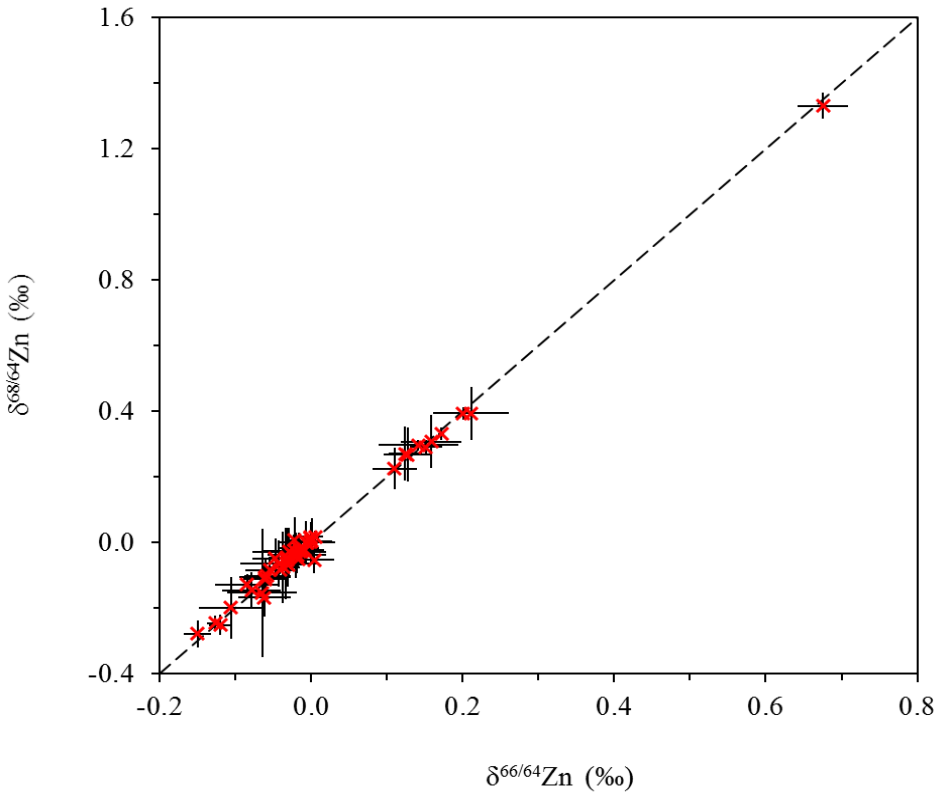

Figure S-2 Plot showing the linear correlation between $\delta^{68/64}Zn$ and $\delta^{66/64}Zn$ in USGS standards and run products including sulphide, silicate, and metal phases. Data are reported in Table S-5.

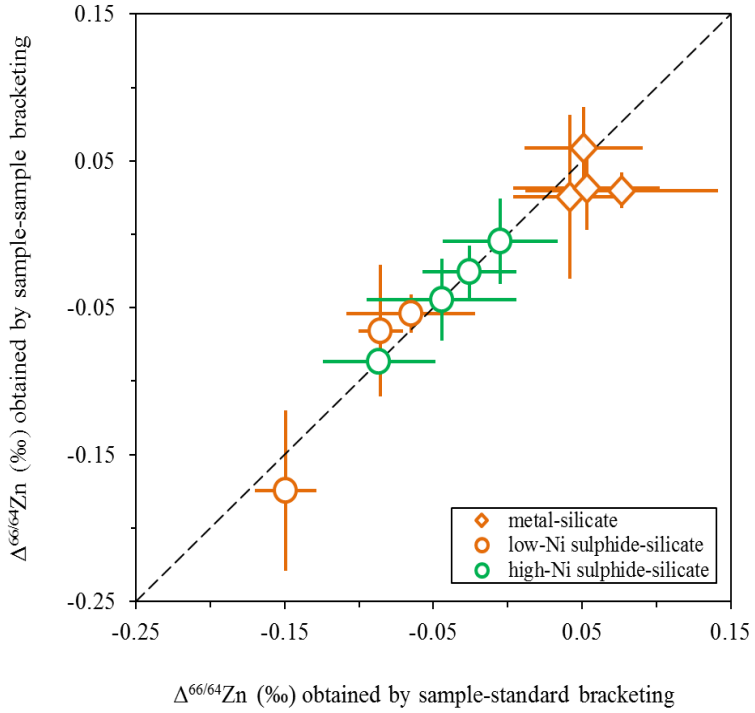

Figure S-3 Comparison of the Zn isotope fractionation factors obtained by conventional sample-standard bracketing and a novel method named as "sample-sample bracketing" (see methods for detail). Data obtained by both methods are identical within errors.

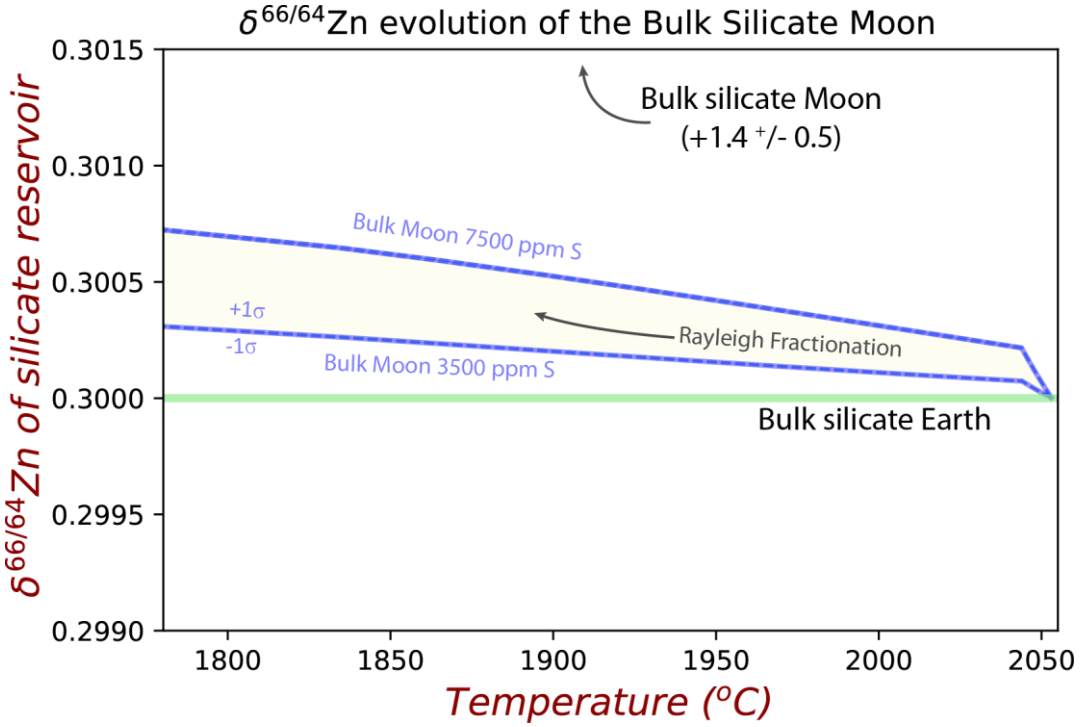

Figure S-4 The silicate Moon's Zn isotope composition is essentially unaffected by lunar sulfide segregation to its core. This assumes the Moon is derived from the precursor BSE, and the Moon's core is predominantly FeS (equating to a bulk Moon of ~7500 ppm S), or just the outer core (3500 ppm S) and sulfide sequestration occurs by Rayleigh fractionation. The green horizontal line represents the values of the BSE (Paniello *et al*., 2012), with lunar values taken from Kato *et al*. (2015). The pale blue band represents 1 standard deviations of the error on the mean of the fractionation regression.

Supplementary Information References

Bridgestock, L., Williams, H., Rehkämper, M., Larner, F., Giscard, M., Hammond, S., Coles, B., Andreasen, R., Wood, B., Theis, K. (2014) Unlocking the zinc isotope systematics of iron meteorites. *Earth and Planetary Science Letters* 400, 153-164.

Chen, S., Liu, Y., Hu, J., Zhang, Z., Hou, Z., Huang, F., Yu, H. (2016) Zinc isotopic compositions of NIST SRM 683 and whole-rock reference Materials. *Geostandards and Geoanalytical Research*.

Craddock, P.R., Warren, J.M., Dauphas, N. (2013) Abyssal peridotites reveal the near-chondritic Fe isotopic composition of the Earth. *Earth and Planetary Science Letters* 365, 63-76.

Danyushevsky, L.V., Plechov, P. (2011) Petrolog3: Integrated software for modeling crystallization processes. *Geochemistry Geophysics Geosystems* 12.

Elardo, S.M., Shahar, A. (2017) Non-chondritic iron isotope ratios in planetary mantles as a result of core formation. *Nature Geoscience* 10, 317-321.

He, Z., Huang, F., Yu, H., Xiao, Y., Wang, F., Li, Q., Xia, Y., Zhang, X. (2016) A flux-free fusion technique for rapid determination of major and trace elements in silicate rocks by LA-ICP-MS. *Geostandards and Geoanalytical Research* 40, 5-21.

Herzog, G., Moynier, F., Albarède, F., Berezhnoy, A. (2009) Isotopic and elemental abundances of copper and zinc in lunar samples, Zagami, Pele's hairs, and a terrestrial basalt. *Geochimica Et Cosmochimica Acta* 73, 5884-5904.

Huang, J., Huang, F., Wang, Z., Zhang, X., Yu, H. (2017) Copper isotope fractionation during partial melting and melt percolation in the upper mantle: Evidence from massif peridotites in Ivrea-Verbano Zone, Italian Alps. *Geochimica Et Cosmochimica Acta* 211, 48-63.

Kato, C., Moynier, F. (2017) Gallium isotopic evidence for extensive volatile loss from the Moon during its formation. *Science Advances* 3, e1700571.

Kato, C., Moynier, F., Valdes, M.C., Dhaliwal, J.K., Day, J.M.D. (2015) Extensive volatile loss during formation and differentiation of the Moon. *Nature Communications* 6, 7617.

Kiseeva, E.S., Wood, B.J. (2013) A simple model for chalcophile element partitioning between sulphide and silicate liquids with geochemical applications. *Earth and Planetary Science Letters* 383, 68-81.

Kiseeva, E.S., Wood, B.J. (2015) The effects of composition and temperature on chalcophile and lithophile element partitioning into magmatic sulphides. *Earth and Planetary Science Letters* 424, 280-294.

Liu, Y., Hu, Z., Gao, S., Günther, D., Xu, J., Gao, C., Chen, H. (2008) In situ analysis of major and trace elements of anhydrous minerals by LA-ICP-MS without applying an internal standard. *Chemical Geology* 257, 34-43.

Mahan, B., Siebert, J., Pringle, E.A., Moynier, F. (2017) Elemental partitioning and isotopic fractionation of Zn between metal and silicate and geochemical estimation of the S content of the Earth's core. *Geochimica Et Cosmochimica Acta* 196, 252-270.

McDade, P., Wood, B.J., Westrenen, W.V., Brooker, R., Gudmundsson, G., Soulard, H., Najorka, J., Blundy, J. (2002) Pressure corrections for a selection of piston-cylinder cell assemblies. *Mineralogical Magazine* 66, 1021-1028.

McDonough, W.F., Sun, S.-s. (1995) The composition of the Earth. *Chemical Geology* 120, 223-253.

Moynier, F., Vance, D., Fujii, T., Savage, P. (2017) The isotope geochemistry of zinc and copper. *Reviews in Mineralogy and Geochemistry* 82, 543-600.

Paniello, R.C., Day, J.M., Moynier, F. (2012) Zinc isotopic evidence for the origin of the Moon. *Nature* 490, 376-9.

Pringle, E.A., Moynier, F. (2017) Rubidium isotopic composition of the Earth, meteorites, and the Moon: Evidence for the origin of volatile loss during planetary accretion. *Earth and Planetary Science Letters* 473, 62-70.

Righter, K., Drake, M.J. (1996) Core Formation in Earth's Moon, Mars, and Vesta. *Icarus* 124, 513-529.

Savage, P.S., Moynier, F., Chen, H., Shofner, G., Siebert, J., Badro, J., Puchtel, I. (2015) Copper isotope evidence for large-scale sulphide fractionation during Earth's differentiation. *Geochemical Perspectives Letters*.

Smythe, D.J., Wood, B.J., Kiseeva, E.S. (2017) The S content of silicate melts at sulfide saturation: new experiments and a model incorporating the effects of sulfide composition. *American Mineralogist* 102, 795-803.

Wade, J., Wood, B.J. (2016) The oxidation state and mass of the Moon-forming impactor. *Earth and Planetary Science Letters* 442, 186-193.

Wang, K., Jacobsen, S.B. (2016) Potassium isotopic evidence for a high-energy giant impact origin of the Moon. *Nature* 538, 487-490.

Weber, R.C., Lin, P.Y., Garnero, E.J., Williams, Q., Lognonne, P. (2011) Seismic detection of the lunar core. *Science* 331, 309-12.

Wood, B.J. (1993) Carbon in the core. *Earth and Planetary Science Letters* 117, 593-607.